Geothermics 91 (2021) 102043

Contents lists available at ScienceDirect

Geothermics

journal homepage: www.elsevier.com/locate/geothermics

Effect of layered geological structures on borehole heat transfer

Sevan Karabetoglu [a], Z. Fatih Ozturk [a], Ayse Kaslilar [b], Christopher Juhlin [b], Altug Sisman [c,*]

[a] Istanbul Technical University, Energy Institute, 34469, Maslak, Istanbul, Turkey
[b] Uppsala University, Department of Earth Sciences, Geophysics, Geocentrum, Villavägen 16, SE-752 36, Uppsala, Sweden
[c] Uppsala University, Department of Physics & Astronomy, Material Theory, Regementsvägen 1, SE-752 37, Uppsala, Sweden

ARTICLE INFO

Keywords:
Borehole heat exchanger
Heat transfer in layered medium
Thermal performance modelling
Deep borehole

ABSTRACT

Borehole heat exchangers, especially deep ones, are usually drilled through different geological layers having varying properties. Homogeneous and layered models can be used for borehole performance predictions. The homogeneous model considers all layers as a single layer having effective properties while the layered model considers all layers separately and gives better accuracy, although it is more complicated and time consuming to calculate. In this study, by considering real geological structures, thermal performance predictions of a deep borehole are made using both homogeneous and layered models and the results are compared to examine how predictions differ from each other depending on the statistical characteristics of geological structures. An analytical expression is derived for the relation between statistical characteristics and deviations from the predictions of the homogeneous model. The magnitudes of deviations are very small and essentially depend on the variance of the difference for the thermal properties of the layers and a time decaying function. The results help to understand how horizontally layered geological structures influence borehole performance and when we need a layered model.

1. Introduction

Environmental sensitivities and high energy prices have increased the interest in energy efficient applications in buildings. Many energy efficient applications have been discussed by many authors using different energy technologies and many different numerical, analytical and experimental analyses have been presented. Also, a large number of books and papers have been published on energy efficient building technologies and regulations (Asdrubali and Desideri, 2018). Furthermore, thermal energy use in private and commercial buildings has been studied to analyze the past, present and future trends as well as how factors in heating and cooling influence energy consumption. Thermal energy consumption can be more than half of the total energy consumption of buildings (Serrano et al., 2017; Ürge-Vorsatz et al., 2015). This important ratio can be reduced by integrating energy efficient and renewable technologies especially during the design phase of the buildings. It is clear that although the physical structure and geographical position of the buildings are the most important factors on energy consumption, the selection of energy efficient heating and cooling equipment is also an important component for cost effective and renewable solutions. Heat pump technologies provide both renewable and energy efficient choices for heating and cooling of buildings. In this technology, depending on seasonal periods, heat energy is extracted from the environment into the buildings or released into the environment. The environment can be air, water or ground, depending on application type and location. It is thermodynamically well known that higher Coefficient of Performance (COP) or Energy Efficiency Ratio (EER) values can be achieved if the source and sink (environment and indoor air) temperatures are close to each other (Rees, 2016), therefore, stable thermal properties and high heat capacity of the underground make ground-source heat pumps (GSHP) advantageous for COP or EER. However, in addition to its many advantages, it is important to note that the long payback time is a significant disadvantage for GSHPs technology. This disadvantage may be reduced to a minimum by considering optimal design criteria (Atam and Helsen, 2016).

GSHP's are easily scaled depending on thermal demands and requirements and generally coupled with horizontal or vertical heat exchangers (GSHE). Therefore, the number of GSHE's may vary from a single one for residential use to even thousands for large scale commercial applications. Thermal performance of GSHE-strongly depends on the thermal properties of the ground and borehole structure. For the proper sizing and optimum system design, thermal properties of the ground must be well known. However, instead of having detailed

* Corresponding author.
E-mail address: altug.sisman@physics.uu.se (A. Sisman).

https://doi.org/10.1016/j.geothermics.2021.102043
Received 20 April 2020; Received in revised form 29 November 2020; Accepted 30 December 2020

Nomenclature

c	volumetric heat capacity ($Jm^{-3}K$)
c_p	specific heat capacity ($Jkg^{-1}K^{-1}$)
$\overline{c}$	mean volumetric heat capacity ($Jm^{-3}K$)
$\widetilde{c}$	dimensionless volumetric heat capacity ($c/\overline{c}$)
G	dimensionless unit heat transfer rate
H	dimensionless heat energy transfer
i	index to denote ith layer
k	thermal conductivity ($Wm^{-1}K^{-1}$)
$\overline{k}$	mean thermal conductivity ($Wm^{-1}K^{-1}$)
$\widetilde{k}$	dimensionless thermal conductivity ($k/\overline{k}$)
N	number of layers
q'	unit heat transfer rate (Wm^{-1})
Q	total heat energy (J)
Q_H	total heat energy for homogenized structure (J)
$\dot{Q}$	total heat energy rate (W)
$\dot{Q}_H$	total heat energy rate for homogenized structure (W)
$\widehat{Q}$	relative transferred heat energy (Q/Q_H)
$\widehat{\dot{Q}}$	relative heat transfer rate ($\dot{Q}/\dot{Q}_H$)
r	radial distance from the center of borehole (m)
r_b	borehole radius (m)
t	operation time of borehole (s)
$\widetilde{t}$	dimensionless operation time, $\widetilde{t} = \alpha t/r_b^2$
$\widetilde{t}_{\overline{\alpha}}$	dimensionless operation time corresponding to mean thermal diffusivity, $\widetilde{t}_{\overline{\alpha}} = \overline{\alpha} t/r_b^2$
T	temperature (°C)
$\overline{T}$	mean temperature (°C)
T_∞	ambient temperature (°C)
z_i	thickness of ith layer (m)
Z	borehole depth (m)

Greek Letters

α	thermal diffusivity (m^2s^{-1})
$\overline{\alpha}$	mean thermal diffusivity (m^2s^{-1})
$\widetilde{\alpha}$	normalized thermal diffusivity
σ_c^2	relative variance of heat capacity (variance over square of mean)
σ_{ck}^2	relative covariance of heat capacity and thermal conductivity (covariance over product of means)
σ_k^2	relative variance of thermal conductivity (variance over square of mean)
σ_{c-k}^2	relative variance of heat capacity and thermal conductivity difference
σ_c^3	relative skewness of heat capacity (skewness over cube of mean)
σ_{cck}^3	relative coskewness of heat capacity square and thermal conductivity (coskewness over product of squared mean of c and mean of k)
σ_k^3	relative skewness of thermal conductivity (skewness over cube of mean)
σ_{kkc}^3	relative coskewness of heat capacity and thermal conductivity square (coskewness over product of squared mean of k and mean of c)
σ_{c-k}^3	relative skewness of heat capacity and thermal conductivity difference
ρ	density (kgm^{-3})

measurements underground, an effective thermal diffusivity definition is generally used in the literature. Effective thermal diffusivity can easily be obtained by using only inlet and outlet temperatures along with volumetric flow rates of the heat exchanger. This widely used and relatively simple technique is named a thermal response test (TRT) (Eskilson, 1987; Mogensen, 1983; Spitler and Gehlin, 2015). By using the effective thermal diffusivity based on the homogenous ground property assumption, thermal properties are considered constant with depth and direction. However, stratified structures may often be present at many locations with variations in the thermo-physical properties changing considerably from one layer to another. Therefore, more advanced TRT models have been proposed by using optical fiber thermometers to get more detailed information in depth throughout the layered underground structure (Acuña, 2013; Fujii et al., 2006, 2009; Sakata et al., 2018). Additionally, accurate determination of thermal properties is particularly important in finding the best design configuration of boreholes in a limited field to prevent thermal shortcuts (Gultekin et al., 2016; Katsura et al., 2008; Kurevija et al., 2011; Law and Dworkin, 2016; Loveridge and Powrie, 2014; Makasis et al., 2018; Yuan et al., 2016). Furthermore, groundwater flows may affect the thermal performance of boreholes (Hecht-Méndez et al., 2013; Meng et al., 2018; Zanchini et al., 2012). Many analytical and numerical models have been developed to calculate the heat transfer rate by considering thermal properties of underground and borehole materials (Yang et al., 2010).

Even for shallow boreholes, GSHEs may pass through many geological layers, therefore, variations in heat transfer between GSHEs and the different layers have become an interesting research topic (Abdelaziz et al., 2014; Erol and François, 2018; Florides et al., 2013; Hu, 2017; Li et al., 2017; Li et al., 2019; Luo et al., 2014; Liu et al., 2020a, b; Pan et al., 2020; Jin et al., 2020). In addition to shallow ones, in recent years, there has been an increase in number of studies, both analytical (Cai et al., 2019; Morchio and Fossa, 2019) and numerical (Luo et al., 2019; Renaud et al., 2019), for modelling of deep boreholes with coaxial pipes. Especially in deep borehole applications, the amount of heat stored/extracted in dissimilar layers may considerably be different from each other, (Liu et al., 2020a). Therefore, the effect of heterogeneity in geological structures on borehole heat transfer may become an important issue. When thermal properties of layers in a formation (thermal profile) are known, the relation between the statistical characteristics of this profile and borehole heat transfer provides a critical information on the effect of the layered structure on the thermal performance of a borehole.

In this study, the relationship between the statistical characteristics of the thermal profile for a given geological structure and the deviations of borehole heat transfer predictions based on a homogenous model is studied. Three different kinds of real geological profiles consisting of horizontal layers are considered and the thermal conditions at different depths of these profiles are studied to simulate different and real heterogeneous ground conditions. In these models, time variations of borehole heat transfer rate as well as heat energy transfer are numerically calculated by using both the homogeneous and layered approaches. The results are compared with each other to analyze the effect of horizontally layered structures on borehole heat transfer. Deviations from the predictions of the homogeneous approach are given. Furthermore, for the first time in the literature, an analytical expression is derived to provide a relation between the statistical characteristics of a geological thermal profile and the deviations of heat transfer predictions from those of a homogeneous model. The results are in good agreement with the numerical ones and provide a concrete formulation and understanding for the behavior of time-dependent heat transfer in boreholes containing horizontally layered geological structures. In contrast, the present results and conclusion may be considerably different for

inclined or vertical layers. Total heat transfer is equal to the sum of the ones in each layer in horizontally layered structures while this is clearly not the case for other configurations. In such cases, different analytical and numerical models are needed.

2. Methods

Analytical and numerical methods are individually used to predict the time dependent thermal performance of a borehole in a layered geological structure by both homogeneous and layered approaches. The ratio of the layered model predictions to those of the homogeneous one is examined for both heat transfer rate and heat energy transfer by considering first an analytical model and then a numerical model. The results of different methods are also compared.

2.1. Analytical model

The heat transfer rate of a borehole in a single homogeneous geological structure can be determined by the axially symmetric transient 1D heat diffusion equation. For constant temperature conditions of the borehole surface, the equation and its initial and boundary conditions are written as follows,

$$\frac{1}{\alpha}\frac{\partial T}{\partial t} = \frac{\partial^2 T}{\partial r^2} + \frac{1}{r}\frac{\partial T}{\partial r} \tag{1a}$$

$$\begin{aligned} T(r,\ 0) &= T_\infty \\ T(r_b, t) &= \overline{T} \\ T(\infty, t) &= T_\infty \end{aligned} \tag{1b}$$

where α is thermal diffusivity of the ground, r and t are radial and time coordinates respectively, T is ground temperature, T_∞ is unperturbed ground temperature and $\overline{T}$ is the mean surface temperature of the borehole with radius r_b (the average fluid temperature). Analytical solution of Eq. (1a) under the conditions of Eq. (1b) is given in the literature (Ozisik, 1993). Therefore, the unit heat transfer rate ($\dot{q}'$, heat power per borehole depth) can be defined in its dimensionless form as,

$$G(\widetilde{t}) = \frac{\dot{q}'}{2\pi k\left(\overline{T} - T_\infty\right)} = \frac{4}{\pi^2}\int_{\beta=0}^{\infty} \frac{e^{-\beta^2 \widetilde{t}}}{\beta\left[\mathrm{J}_0^2(\beta) + \mathrm{Y}_0^2(\beta)\right]} d\beta \tag{2}$$

where k is the thermal conductivity of the ground, J_0 and Y_0 are the first and the second kind of zeroth order Bessel functions respectively and $\widetilde{t}$ is the dimensionless operation time defined as $\widetilde{t} = t/\tau = \alpha t/r_b^2$. For a homogenous structure, the total heat transfer rate of a borehole is then simply expressed as,

$$\dot{Q}(t) = 2\pi\left(\overline{T} - T_\infty\right) Z\, k\, G(\widetilde{t}) \tag{3}$$

where Z stands for the total borehole depth. By integrating Eq. (3) over the operation time t, the total heat energy transfer is calculated as,

$$Q(t) = \int_0^t \dot{Q}(t')dt' = 2\pi r_b^2 Z\left(\overline{T} - T_\infty\right)\ c\, H(\widetilde{t}) \tag{4}$$

where $c = \rho c_p$ is the volumetric heat capacity of the ground and $H(\widetilde{t})$ is the dimensionless heat energy transfer defined as,

$$H(\widetilde{t}) = \frac{4}{\pi^2}\int_{\beta=0}^{\infty} \frac{1 - e^{-\beta^2 \widetilde{t}}}{\beta^3\left[\mathrm{J}_0^2(\beta) + \mathrm{Y}_0^2(\beta)\right]} d\beta \tag{5}$$

In the case of a layered structure, the total heat transfer rate can be expressed as a summation of the rates in each layer if heat transfer between successive layers are negligible, which is usually the case in the ground. In the numerical model section, we calculate the contribution of interlayer heat transfer and show that it is almost completely negligible (around 0.1 %). A schematic view of a borehole in a layered geological structure consisting of N layers is given in Fig. 1. For the layer i having thickness of z_i, the heat transfer rate is written by Eq. (3) as,

$$\dot{Q}_i = 2\pi\left(\overline{T} - T_\infty\right) z_i k_i G\left[\widetilde{t}_i(\alpha_i)\right] \tag{6}$$

Summing Eq. (6) over all layers, the total heat transfer rate is obtained as,

$$\dot{Q} = 2\pi\left(\overline{T} - T_\infty\right) \sum_{i=1}^{N} z_i k_i G\left[\widetilde{t}_i(\widetilde{\alpha}_i)\right] \tag{7}$$

On the other hand, homogenized (averaged or effective) ground properties can easily be obtained just by weighted averaging of the layer properties over their thicknesses. Therefore, the total heat transfer rate in a homogeneous approach can simply be written as follows

$$\dot{Q}_H = 2\pi\left(\overline{T} - T_\infty\right) Z\overline{k}\, G(\widetilde{t}_{\overline{\alpha}}) \tag{8}$$

where $\overline{k}$ is the mean thermal conductivity defined as $\overline{k} = \sum_{i=1}^{N} k_i \widetilde{z}_i$ with $\widetilde{z}_i = z_i/Z$ and total number of layers N. Similarly $\overline{\alpha} = \overline{k}/\overline{c}$ is defined as the mean thermal diffusivity in terms of mean thermal conductivity and mean volumetric heat capacity ($\overline{c}$), $\widetilde{t}_{\overline{\alpha}}$ is the dimensionless time calculated for mean thermal diffusivity. The relationship between the dimensionless time for the properties of layer i and the one for averaged thermal diffusivity is,

$$\widetilde{t}_i = \widetilde{\alpha}_i \widetilde{t}_{\overline{\alpha}} \tag{9}$$

where; $\widetilde{\alpha}_i = \alpha_i/\overline{\alpha}$ is the normalized thermal diffusivity with $\alpha_i = k_i/\left(\rho c_p\right)_i = k_i/c_i$. Similarly, $\widetilde{k}_i = k_i/\overline{k}$ and $\widetilde{c}_i = c_i/\overline{c}$ are defined as normal-

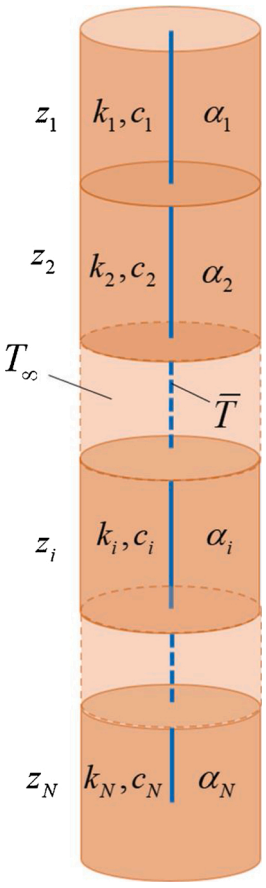

Fig. 1. A layered geological structure consisting of N layers having different thermal properties and thicknesses.

ized thermal conductivity and normalized volumetric heat capacity of the *i*th layer respectively.

Furthermore, by using the definitions of normalized properties, it is easy to see that,

$$\sum_{i=1}^{N}\widetilde{k}_i=\sum_{i=1}^{N}\widetilde{c}_i=\sum_{i=1}^{N}\widetilde{\alpha}_i=1 \tag{10}$$

To examine the cost of the homogeneous approach, the ratio of true heat transfer rate, Eq. (7), to the homogenized one, Eq. (8), is considered as follows,

$$\widehat{Q}=\frac{\dot{Q}}{\dot{Q}_H}=\sum_{i=1}^{N}\widetilde{z}_i\widetilde{k}_i\, r_G\left(\widetilde{\alpha}_i\widetilde{t}_{\widetilde{\alpha}}\right) \tag{11}$$

where; $r_G\left(\widetilde{t}_{\widetilde{\alpha}}\widetilde{\alpha}_i\right)$ is given by

$$r_G\left(\widetilde{t}_{\widetilde{\alpha}}\widetilde{\alpha}_i\right)=\frac{G\left(\widetilde{t}_{\alpha_i}\right)}{G\left(\widetilde{t}_{\widetilde{\alpha}}\right)}=\frac{\int_{\beta=0}^{\infty}\frac{e^{-\beta^2\widetilde{t}_{\widetilde{\alpha}}\widetilde{\alpha}_i}}{\beta\left[\mathrm{J}_0^2(\beta)+\mathrm{Y}_0^2(\beta)\right]}d\beta}{\int_{\beta=0}^{\infty}\frac{e^{-\beta^2\widetilde{t}_{\widetilde{\alpha}}}}{\beta\left[\mathrm{J}_0^2(\beta)+\mathrm{Y}_0^2(\beta)\right]}d\beta} \tag{12}$$

Eq. (12) represents the time evolution of the relative heat transfer rate, $\widehat{Q}$, for each layer. In order to derive the functional dependency of the relative heat transfer rate on the statistical parameters of a layered structure, a Taylor series expansion is applied to Eq. (11) by considering the terms depending on $\widetilde{k}_i$ and $\widetilde{c}_i$. The term containing these variables in Eq. (11) is represented by the Taylor expansion as,

$$\widetilde{k}_i\exp\left(-\beta^2\widetilde{t}_{\widetilde{\alpha}}\frac{\widetilde{k}_i}{\widetilde{c}_i}\right)=\lim_{W\to\infty}\sum_{n=0}^{W}\times\sum_{m=0}^{W-n}\left[\frac{d^{(n+m)}}{d\widetilde{k}_i^{n}d\widetilde{c}_i^{m}}\widetilde{k}_i\exp\left(-\beta^2\widetilde{t}_{\widetilde{\alpha}}\frac{\widetilde{k}_i}{\widetilde{c}_i}\right)\right]\Bigg|_{\substack{\widetilde{k}_i=1\\ \widetilde{c}_i=1}}\frac{\left(\widetilde{k}_i-1\right)^n(\widetilde{c}_i-1)^m}{n!m!} \tag{13a}$$

By neglecting third and higher order terms;

$$\widetilde{k}_i\exp\left(-\beta^2\widetilde{t}_{\widetilde{\alpha}}\frac{\widetilde{k}_i}{\widetilde{c}_i}\right)\approx\exp\left(-\beta^2\widetilde{t}_{\widetilde{\alpha}}\right)\left[\begin{array}{l}\widetilde{k}_i+\beta^2\widetilde{t}_{\widetilde{\alpha}}\left[(\widetilde{c}_i-1)-\left(\widetilde{k}_i-1\right)\right]-\left(\beta^2\widetilde{t}_{\widetilde{\alpha}}-\frac{\beta^4\widetilde{t}_{\widetilde{\alpha}}^2}{2}\right)\left[(\widetilde{c}_i-1)^2+\left(\widetilde{k}_i-1\right)^2\right]\\ +2\left(\beta^2\widetilde{t}_{\widetilde{\alpha}}-\frac{\beta^4\widetilde{t}_{\widetilde{\alpha}}^2}{2}\right)(\widetilde{c}_i-1)\left(\widetilde{k}_i-1\right)\end{array}\right] \tag{13b}$$

Substituting Eq. (13b) into Eq. (11), the relative heat transfer rate, $\widehat{Q}$ can be expressed as,

$$\widehat{Q}=\sum_{i=1}^{N}\widetilde{z}_i\left[\begin{array}{l}\widetilde{k}_ig_0+\left[(\widetilde{c}_i-1)-\left(\widetilde{k}_i-1\right)\right]g_1-\left[(\widetilde{c}_i-1)^2+\left(\widetilde{k}_i-1\right)^2\right](g_1-g_2)\\ +2(\widetilde{c}_i-1)\left(\widetilde{k}_i-1\right)(g_1-g_2)\end{array}\right] \tag{14}$$

where the *g* function with order of *m* is given as,

$$g_m\left(\widetilde{t}\right)=\frac{\widetilde{t}_{\widetilde{\alpha}}^m}{m!}\frac{\int_{\beta=0}^{\infty}\frac{\beta^{2m}e^{-\beta^2\widetilde{t}_{\widetilde{\alpha}}}}{\beta\left[\mathrm{J}_0^2(\beta)+\mathrm{Y}_0^2(\beta)\right]}d\beta}{\int_{\beta=0}^{\infty}\frac{e^{-\beta^2\widetilde{t}_{\widetilde{\alpha}}}}{\beta\left[\mathrm{J}_0^2(\beta)+\mathrm{Y}_0^2(\beta)\right]}d\beta} \tag{15}$$

Clearly, from Eq. (15), $g_0=1$. Besides, due to the relations of

$$\sum_{i=1}^{N}\widetilde{z}_i=\sum_{i=1}^{N}\widetilde{z}_i\widetilde{k}_i=\sum_{i=1}^{N}\widetilde{z}_i\widetilde{c}_i=1 \tag{16}$$

the second term in the outer square bracket of Eq. (14) vanishes and the expression simplifies as,

$$\begin{aligned}\widehat{Q}&=1-(g_1-g_2)\sum_{i=1}^{N}\widetilde{z}_i\left[(\widetilde{c}_i-1)-\left(\widetilde{k}_i-1\right)\right]^2\\&=1-(g_1-g_2)\left(\sigma_c^2+\sigma_k^2-2\sigma_{ck}^2\right)=1-(g_1-g_2)\sigma_{c-k}^2\end{aligned} \tag{17}$$

where; $\sigma_c^2,\sigma_k^2,\sigma_{ck}^2$ and σ_{c-k}^2 are the statistical parameters of the thermal property profile of the structure, namely normalized variances of *c* and *k* as well as their normalized covariance and variance of difference, respectively. Definitions of $\sigma_c^2,\sigma_k^2,\sigma_{ck}^2$ and σ_{c-k}^2 are given as follows by considering Eq. (16),

$$\sigma_c^2=\sum_{i=1}^{N}\widetilde{z}_i(\widetilde{c}_i-1)^2=\sum_{i=1}^{N}\widetilde{z}_i\left(\widetilde{c}_i^2-2\widetilde{c}_i+1\right)=\sum_{i=1}^{N}\widetilde{z}_i\widetilde{c}_i^2-1 \tag{18a}$$

$$\sigma_k^2=\sum_{i=1}^{N}\widetilde{z}_i\left(\widetilde{k}_i-1\right)^2=\sum_{i=1}^{N}\widetilde{z}_i\left(\widetilde{k}_i^2-2\widetilde{k}_i+1\right)=\sum_{i=1}^{N}\widetilde{z}_i\widetilde{k}_i^2-1 \tag{18b}$$

$$\sigma_{ck}^2=\sum_{i=1}^{N}\widetilde{z}_i(\widetilde{c}_i-1)\left(\widetilde{k}_i-1\right)=\sum_{i=1}^{N}\widetilde{z}_i\left(\widetilde{c}_i\widetilde{k}_i-\widetilde{c}_i-\widetilde{k}_i+1\right)=\sum_{i=1}^{N}\widetilde{z}_i\widetilde{c}_i\widetilde{k}_i-1 \tag{18c}$$

$$\sigma_{c-k}^2=\sigma_c^2+\sigma_k^2-2\sigma_{ck}^2 \tag{18d}$$

Eqs. (18a)–(18d) can even be expressed in more simplified forms. The details are given in Appendix A.

By applying similar mathematical processes, the expression of relative heat energy transfer based on the second order approach can be obtained as,

$$\begin{aligned}\widehat{Q}=\frac{Q}{Q_H}&=1-h_2\sum_{i=1}^{N}\widetilde{z}_i\left[(\widetilde{c}_i-1)-\left(\widetilde{k}_i-1\right)\right]^2=1-h_2\left(\sigma_c^2+\sigma_k^2-2\sigma_{ck}^2\right)\\&=1-h_2\sigma_{c-k}^2\end{aligned} \tag{19}$$

where, the *h* function with order of *m* is given as,

$$h_m\left(\widetilde{t}\right)=\frac{\widetilde{t}_{\widetilde{\alpha}}^m}{m!}\frac{\int_{\beta=0}^{\infty}\frac{\beta^{2m}e^{-\beta^2\widetilde{t}_{\widetilde{\alpha}}}}{\beta^3\left[\mathrm{J}_0^2(\beta)+\mathrm{Y}_0^2(\beta)\right]}d\beta}{\int_{\beta=0}^{\infty}\frac{1-e^{-\beta^2\widetilde{t}_{\widetilde{\alpha}}}}{\beta^3\left[\mathrm{J}_0^2(\beta)+\mathrm{Y}_0^2(\beta)\right]}d\beta} \tag{20}$$

Eqs. (15) and (20) represent the time evolution of relative heat transfer rate and heat energy transfer, respectively. The contribution of the higher order statistical parameters can be neglected since the second order terms are quite sufficient for the analysis targeted here as well as for most of the practical cases. On the other hand, the third order representations of Eqs. (17) and (19) are given in Appendix B to give an idea about how these expressions become unfriendly to use even for the third order.

Dimensionless time dependencies of g_1-g_2 and h_2 in Eqs. (17) and (19) are given in Fig. 2. For the usual values of the ground's thermal diffusivity and borehole radius, $\tau=r_b^2/\alpha$ takes the values in the ranges of 5000 s and 10,000 s (1.4 h – 2.8 h). Thus, the value of $\widetilde{t}=1400$ usually

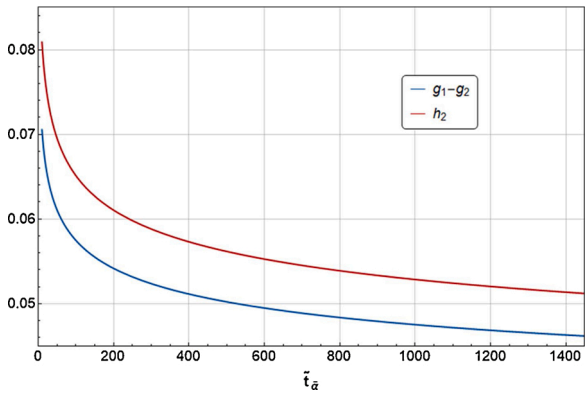

Fig. 2. Time dependencies of g_1–g_2 (the curve below in B&W version) and h_2 functions.

corresponds to 2000 h – 4000 h of non-stop operation time (approx. 3–6 months). Therefore, the dimensionless time range in Fig. 2 involves a very wide range of GSHP applications under the worst case scenario (non-stop operation).

The mean values of $g_1 - g_2$ and h_2 functions over the whole operational time range are around 0.050 and 0.056 respectively. Therefore, by considering Eqs. (17) and (19), it is possible to say that time variations of $\widehat{Q}$ and $\widehat{Q}$ are in the order of 5% and 6% of the value of σ^2_{c-k}. A criticism about the order of magnitudes of $\widehat{Q}$ and $\widehat{Q}$ is given in discussion section.

2.2. Numerical model

To compare the analytical results, a numerical model, which considers also axial heat transfer between successive layers, is established in the finite element based COMSOL® Multiphysics Modelling Software environment. A GSHE is simulated by considering a single borehole having a radius of 0.1 m and constant surface temperature of 2 °C. Both initial and ambient temperatures of the ground are chosen as 17 °C. Borehole depth is 750 m and it is surrounded by a ground having several geological layers with different thermal properties and thicknesses. A sample sketch is shown in Fig. 3. Different thermal properties of the layers cause different heat transfer rates in each layer. Therefore, the temperature field becomes different in each successive layer as long as their thermal properties are different. As a result of this process, axial heat transfer first develops at the interfaces of these layers and then decays with time. Depending on the time and space variations of this axial heat transfer, the effect of the layered geological structure on the borehole heat transfer becomes quite complicated. Therefore, the 2D axially symmetric transient heat diffusion equation is solved.

For the verification of the numerical model, the heat transfer rate predictions for a homogenized domain are compared with those of the analytical model based on the assumption of a constant cylindrical surface temperature of 2 °C. Thermal properties of sandstone are used ($k = 3.52$ W/mK, $c = 1.94$ MJ/m^{3}K), as a sample case, both in the analytical and numerical models. The numerical and analytical predictions for the time evaluation of heat transfer rate match each other with less than 0.4 % mean absolute percentage error (MAPE) for the range of $\tilde{t} = 5 - 1400$. Furthermore, the numerical model is also verified for the homogenized approach by comparing its heat transfer rate predictions with the experimental measurements for a 50 m deep borehole with a single U-tube in the application field of Istanbul Technical University Ground Source Heat Pump Laboratory. In the application field, thermal properties of the ground are almost homogenous and the numerical model gives the results which are very close to those of 70 h of measurements, with a MAPE value less than 1.6 % (Aydin and Sisman, 2015).

Three different layered geological models (called case-A, B and C) consisting of distinct combinations of five different geological units are considered as a heat transfer medium. The structure of these geological models are given in Table 1 and they are based on real data provided in (Ivanova et al., 2013). Thermal properties of the geological units (thermal conductivity k; density ρ; specific heat c_p; volumetric heat capacity c; and thermal diffusivity α) are also summarized in Table 2. The horizontal red lines in Table 1, from top to bottom, indicate the different depths of 150 m, 450 m and 750 m respectively. In each model, three different depths (150 m, 450 m and 750 m) are considered in order to investigate the depth dependence of deviations in the homogeneous model predictions from the layered (heterogeneous) one. Note that all boreholes have a total depth of 750 m.

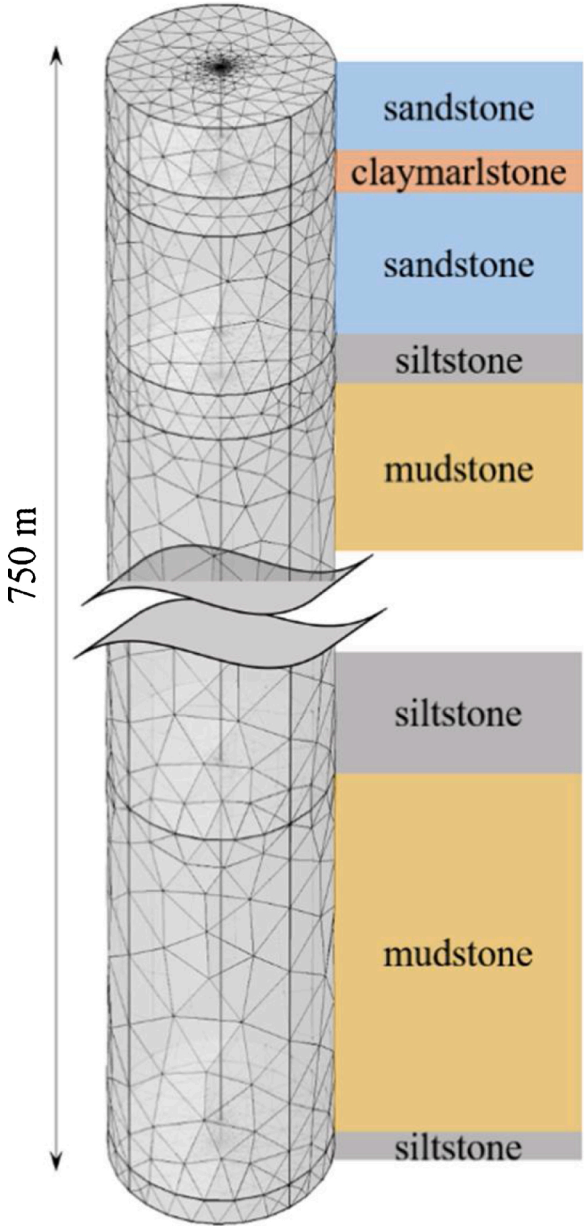

Fig. 3. A sample sketch of a computational model for the GSHE in a layered geological structure.

Numerical calculations are made using both the layered and homogeneous approaches. In the homogeneous approach, the ground is considered as a single homogenized layer. To find the mean thermal properties of this homogenized (effective) layer, the properties of each layer are weighted by using its thickness. In contrast, in the layered model, the layers given in Table 1 are considered.

Table 1
Distribution of geological units in three different cases (profiles) for computational modelling. Horizontal red lines from top to bottom indicate the depths of 150 m, 450 m and 750 m respectively (For interpretation of the references to colour in this Table legend, the reader is referred to the web version of this article.).

Case A		Case B		Case C	
Δz [m]	Geological units	Δz [m]	Geological units	Δz [m]	Geological units
51	sandstone	18	sandstone	59	sandstone
98	mudstone	7	claymarlstone	90	mudstone
1	siltstone	28	sandstone	1	siltstone
109	siltstone	85	mudstone	26	siltstone
37	mudstone	12	siltstone	10	sandstone
4	sandstone	17	siltstone	25	mudstone
66	sandstone	9	sandstone	49	siltstone
77	siltstone	22	mudstone	10	sandstone
7	mudstone	48	siltstone	12	mudstone
44	mudstone	11	sandstone	18	sandstone
36	claymarlstone	19	mudstone	5	sandstone
6	anhydrite	14	siltstone	10	siltstone
31	claymarlstone	10	sandstone	53	sandstone
15	mudstone	37	sandstone	25	mudstone
13	claymarlstone	29	mudstone	20	sandstone
5	sandstone	20	sandstone	23	siltstone
25	sandstone	34	siltstone	14	mudstone
37	mudstone	30	mudstone	110	mudstone
32	claymarlstone	71	mudstone	15	anhydrite
56	anhydrite	14	anhydrite	25	mudstone
		65	mudstone	150	mudstone
		14	mudstone		
		23	sandstone		
		113	mudstone		

After the time dependent temperature field is solved for, the total heat transfer rate is calculated by integrating the normal conductive heat flux over the borehole surface. Also the heat energy transfer between the GSHE and the surrounding ground is determined by time integration of the total heat transfer rate over the operation time, *t*. A free triangular mesh structure is chosen and edited manually by user controlled in the meshing option. The degrees of freedom values vary from 42,000 to 210,000 depending on the depths of the cylindrical domains such as 150 m, 450 m and 750 m. Dense meshing is applied near the borehole surface by reducing the mesh size.

The numerical calculations show that the relative contribution of axial heat transfers between the layers to the borehole's heat transfer rate is about 0.1 %. For case C as an example, the unit heat transfer rates at the end of 2400 h are obtained as 48.24 W/m and 48.18 W/m when the axial heat transfer is considered and ignored respectively. In fact, it is completely negligible for all the cases considered here and this is valid for almost all reasonable geological structures.

Another consideration is the possible effect of initial ground temperature profile on the relative heat transfer rate as well as heat energy transfer. When a deep borehole is considered, initial temperature of ground is not a constant, but instead, it linearly increases with depth (around 0.02−0.03 °C/m). Therefore, temperature difference between the fluid and ground changes with depth and this leads also the unit heat transfer rate to change with depth. This behavior is naturally valid for both in homogeneous and layered geological structures.

On the other hand, temperature difference can be changed also by flow velocity of the fluid. There are two possible limits. At low flow velocity limit, the fluid temperature almost follows the ground temperature changes with depth while it stays constant at high velocity limit and causes an increment in temperature difference between the fluid and ground at deeper parts. However, the effect of temperature gradient should expect to be extremely small since we examine the relative heat transfer rate. Because the effects of ground temperature gradient on heat transfer rates in layered and homogeneous structures are almost the same and they practically cancel each other when the ratio of heat transfer rates is considered.

In our preliminary numerical model, we considered 0.03 °C/m temperature gradient and saw that the effect of temperature gradient on the relative heat transfer rate is completely negligible in case of low flow velocity limit (less than 0.001 %) while it is in the order of 0.5 % for high velocity limit. Consequently, the same equation and conditions, Eqs. (1a) and (1b), of the analytical model are considered for each layer also in the numerical model for further calculations to make the model results comparable with the analytical ones.

Before the comparison of the analytical and numerical results, we need the statistical characteristics of each layered model (A, B and C) for each depth group (i.e. 150 m, 450 m and 750 m) in Table 1. Thermal properties of the different geological units of the profiles, given in Table 1, are taken from Table 2. The statistical characteristics for several depth groups are then calculated by using Eqs. (18a)–(18d) and given in Table 3

For the calculation of the values in Table 3, Eqs. (A1a)–(A1d) can also be used. It is seen that the values of σ_c^2 are much smaller than those of σ_k^2, except for the cases of A-150 m and C-150 m. This is an expected result since the variation of volumetric heat capacity of the different geological units are small in comparison with that of the thermal conductivity in general, see also Table 2. For the cases of A-150 m and C-150 m, both σ_k^2 and σ_c^2 are very small since the geological structures consist of almost only sandstone and mudstone (see Table 1) which have very similar heat conductivity and heat capacity values, Table 2. Note that this is not the case for B-150 m since it contains also the siltstone which has considerably different thermal conductivity than that of the others components. Similarly, σ_{ck}^2 shows negligibly small values since the correlation between volumetric heat capacity and thermal conductivity of the geological materials is very weak. As a result, except for the cases of A-150 m and C-150 m where the values of σ_{c-k}^2 are already negligible, σ_{c-k}^2 values are approximately in the order of σ_k^2, $\sigma_{c-k}^2 \approx \sigma_k^2$, as seen in Table 3.

3. Results

Comparisons of the analytical and numerical predictions for both the relative heat transfer rate and the heat energy transfer are given in Figs. 4–6 for the three different cases. Solid curves represent the analytical model predictions while the dashed ones stand for those of the numerical model. Blue, green and red colors are chosen to denote the depths of 150 m, 450 m and 750 m respectively. The analytical and numerical results are in good agreement for all cases. Note that the analytical results are based on Eqs. (17) and (19) which include only the second order terms to keep the expressions as simple as possible. This second order approach is one of the reasons for the differences between the analytical and numerical results. Another reason is the numerical truncations during the computational calculations. By considering both higher order approaches in the analytical expressions and higher precisions in the computational calculations, these small differences can even be made smaller. Nevertheless, the difference is already very small and there is no need to increase the order of approximation of the analytical expressions, which makes them unnecessarily complicated and difficult to use, like the ones given in Appendix B, Eqs. (B3) and (B4).

Figs. 4–6 show that the deviations of both $\hat{\hat{Q}}$ and $\hat{Q}$ from the unit value are almost the same. Eqs. (17) and (19) explain the reason for this behavior. Both of them depend on the same value of σ_{c-k}^2 and the only difference between $\hat{\hat{Q}}$ and $\hat{Q}$ comes from the difference between g_1-g_2 and h_2 which is in the order of 10 %, Fig. 2.

Another result of Figs. 4–6 is that $\hat{\hat{Q}}$ and $\hat{Q}$ take the values nearest to

Table 2
Thermophysical properties of different geological units in Table 1, (Eppelbaum et al., 2014; Fuchs et al., 2015; Labus and Labus, 2018; Schärli and Rybach, 2001) (For interpretation of the references to colour in this Table legend, the reader is referred to the web version of this article.).

Geological units	k [W/mK]	ρ [kg/m^3]	c_p [J/kgK]	ρc_p[MJ/m^{3}K]	α [x10^{-6} m^2/s]
SandStone	3.52	2300	845	1.94	1.811
SiltStone	2.22	2550	795	2.02	1.095
MudStone	3.34	2630	830	2.18	1.530
Claymarlstone	2.14	2500	858	2.14	0.997
Anhydrite	4.85	2960	585	1.73	2.801

Table 3
Statistical characteristics of the geological structures, given in Table 1, for different depths.

Cases-Depths	σ_k^2	σ_c^2	σ_{ck}^2	σ_{c-k}^2
A-150 m	0.001432	0.002913	−0.001271	0.006887
A-450 m	0.041677	0.002092	0.001172	0.041424
A-750 m	0.068526	0.004209	−0.008550	0.089834
B-150 m	0.016034	0.002711	−0.000744	0.020233
B-450 m	0.032386	0.002469	0.000743	0.033369
B-750 m	0.024716	0.002869	−0.000502	0.028589
C-150 m	0.001476	0.003130	−0.001373	0.007352
C-450 m	0.028009	0.002623	−0.000134	0.030899
C-750 m	0.021523	0.003031	−0.000921	0.026398

unity for all cases with 150 m depth although the order of magnitudes differ for different cases when the deeper parts (450 m and 750 m) are considered. For the layers within 150 m depth, the amounts of mudstone and sandstone are almost the same in all cases. This explains why the smallest values of σ_{c-k}^2 in Table 3 appear for 150 m and cause the highest values of $\hat{\hat{Q}}$ and $\hat{Q}$ in Figs. 4–6. In Fig. 7, the weight distributions of geological units in different cases are also given for different depths to make the comparisons easy.

In case of 450 m, considerable amount of siltstone is also included to the bunch of mudstone and sandstone layers. This causes more heterogeneity and the smaller values for $\hat{\hat{Q}}$ and $\hat{Q}$ in comparison with the values for 150 m, Figs. 4 and 5. Tables 1 and 3 and Fig. 7 clearly support this explanation.

For 750 m depths, the magnitudes of $\hat{\hat{Q}}$ and $\hat{Q}$ for Cases B and C are different from those for Case A. This is because the structural heterogeneity of Case A is higher than those of Cases B and C, as it is seen in Table 1 and Fig. 7. We can see the same situation also from the statistical parameters in Table 3. Especially, the geological units of Cases B and C in between 450 m–750 m consist of almost only mudstone since the thicknesses of the anhydrite and sandstone units are negligible while this is not the case for Case A. Therefore, both $\hat{\hat{Q}}$ and $\hat{Q}$ values are closer to the unity in Cases B and C, Figs. 5 and 6 respectively, in comparison with

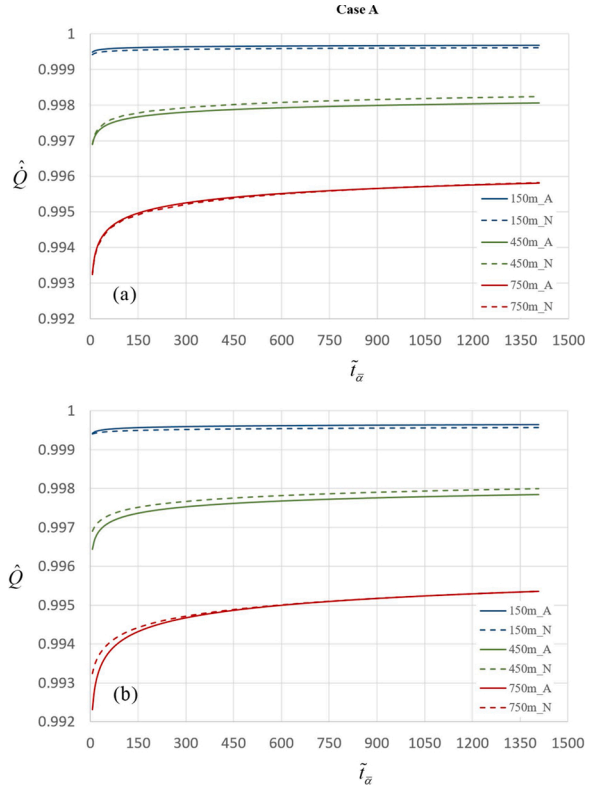

Fig. 4. Comparison of analytical and numerical results for both relative heat transfer rates (a) and heat energy transfer (b) for Case A. Solid curves represent analytical results while the dashed ones stand for the numerical ones. For B&W version, the curves from above to below in each graph correspond to 150 m, 450m and 750 m respectively.

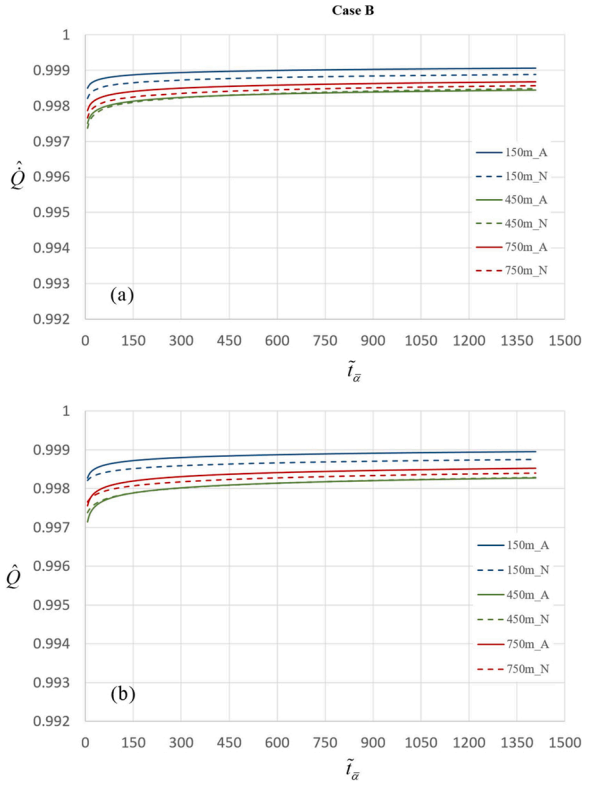

Fig. 5. Comparison of analytical and numerical results for both relative heat transfer rates (a) and heat energy transfer (b) for Case B. Solid curves represent analytical results while the dashed ones stand for the numerical ones. For B&W version, the curves from above to below in each graph correspond to 150 m, 750m and 450 m respectively.

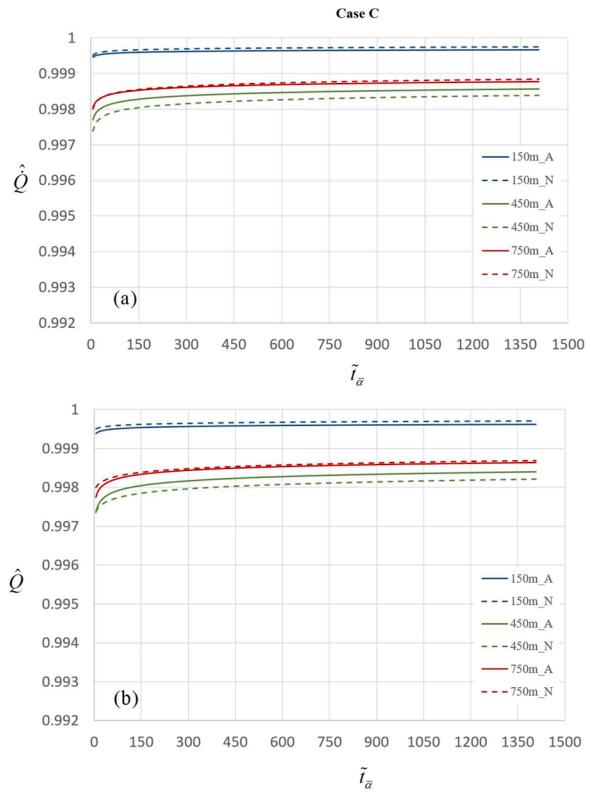

Fig. 6. Comparison of analytical and numerical results for both relative heat transfer rates (a) and heat energy transfer (b) for Case C. Solid curves represent analytical results while the dashed ones stand for the numerical ones. For B&W version, the curves from above to below in each graph correspond to 150 m, 750m and 450 m respectively.

Case A represented by Fig. 4.

For a given geological structure, $\hat{\hat{Q}}$ and $\hat{Q}$ are usually expected to be inversely proportional with depth since the statistical parameters (variance and covariance) are expected to take higher values when more and more different layers are involved. This is why the order of magnitude of the curves in Fig. 4 is in the order of 150 m, 450 m and 750 m. On the other hand, this is true only for Case A. Because the values of $\hat{\hat{Q}}$ and $\hat{Q}$ for 750 m are smaller than those of 450 m for Cases B and C. This result can easily be predicted and explained by Eqs. (17) and (19) together with the values in Table 3. The same result can also directly be predicted from Fig. 7 as it is seen that the heterogeneities of 450 m are higher than those of 750 m for Cases B and C. In other words, the amounts of geological units in Cases B and C are almost evenly distributed in 450 m configurations while the mudstone becomes highly dominant and makes the medium more homogeneous in case of 750 m.

4. Discussion and conclusions

We see that the analytical expressions derived and presented here are able to explain and predict all behaviors of $\hat{\hat{Q}}$ and $\hat{Q}$ in a simpler manner. Therefore, without establishing complicated numerical models for layered structures and making time consuming computational calculations, it is possible to get the same results just by using a simple homogenized computational or even analytical model and then correcting the results by Eqs. (17) and (19).

Another significant contribution of these equations is to explain how and how much heterogeneity (represented by statistical parameters) of the geological structures affect both the heat transfer rate and the heat energy transfer when they are compared with the ones in the homogenized (mixed as a single layer) structure. Therefore, the predictions of a simple homogenized model can easily be used to predict the true values and also to understand whether the horizontally layered structure causes a considerable difference in thermal performance of a borehole heat exchanger. Eqs. (17) and (19) infer that the predictions of the heterogeneous model are always lower than the homogenized model predictions since σ^2_{c-k} is a positive definite quantity.

Furthermore, we see that unless the value of σ^2_{c-k} is not extremely high, the homogenized model gives almost the same results as the heterogeneous one. In other words, the ground's effective (homogenized) thermal parameters, like effective thermal conductivity and volumetric heat capacity, determined by the usual thermal response tests (TRT) can quite be sufficient to predict the true thermal behaviors of ground heat

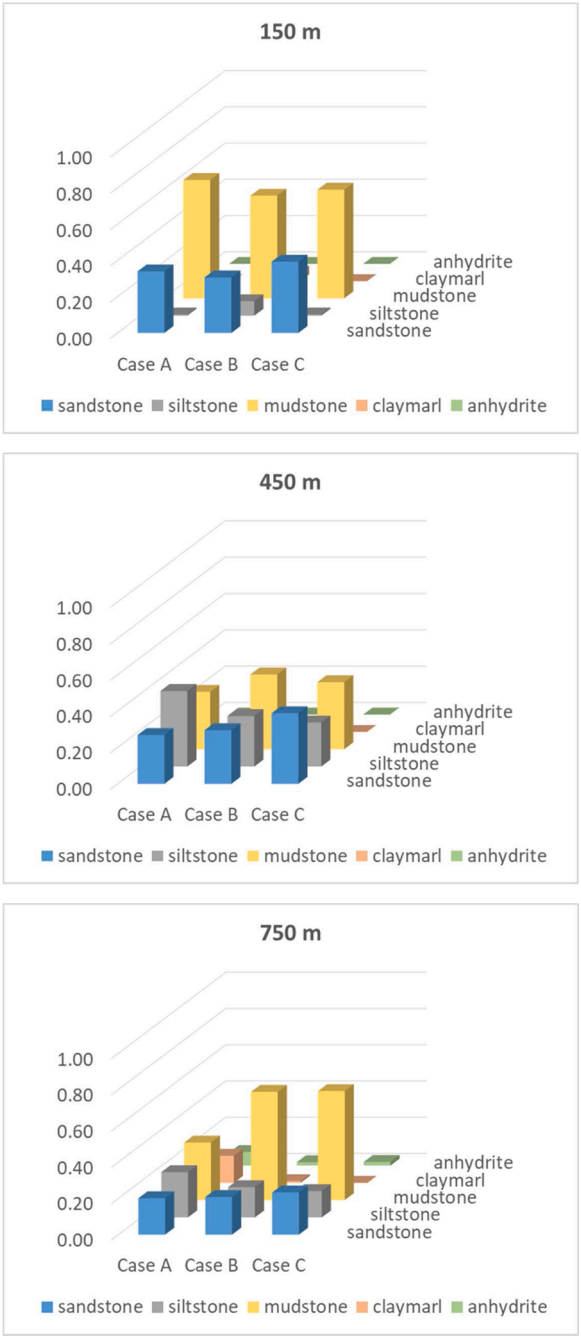

Fig. 7. Visual comparisons of the weight distributions (dominances) of geological units for different cases and depths. The weights are calculated by using the values of thicknesses of layers given in Table 1, as the ratio of total thickness of a specific unit to the total depth.

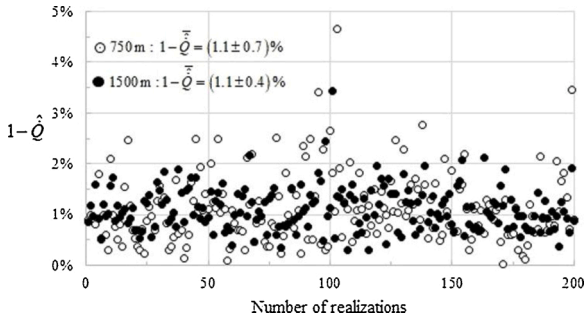

Fig. 8. Deviations of homogenized model predictions for randomly generated and horizontally layered geological structures of 750 m and 1500 m depths.

exchangers in a layered geological structure just by using a homogenous model.

Eq. (A1d) in Appendix A provides an even simpler and easier formulation to calculate σ^2_{c-k} to be used in Eqs. (17) and (19) for the determination of the deviations from the homogenized model, $\hat{\hat{Q}}$ and $\hat{Q}$. In this study, three different geological depth profiles obtained from real data are considered and both analytical and numerical calculations are made for these profiles to investigate the relationship of σ^2_{c-k} with $\hat{\hat{Q}}$ and $\hat{Q}$. However, due to the complex nature of the subsurface geological depth profiles may consist of considerably different geological units having a wide range of thicknesses and thermal properties. In other words, the more geological depth profiles are needed to be studied for better understanding of their effects on σ^2_{c-k} as well as $\hat{\hat{Q}}$ and $\hat{Q}$. For this purpose, four hundred different geological depth profiles consisting of a random number of horizontal layers having different thicknesses (1−200 m), thermal conductivities (0.5–4.5 W/mK) and volumetric heat capacities (1.7–2.7 MJ/m^{3}K) are synthetically generated. In this way, σ^2_{c-k} is calculated for each random geological depth profile by considering two different depths, 750 m and 1500 m, to examine the variation of $1-\hat{\hat{Q}} = (g_1 - g_2)\sigma^2_{c-k}$ for different depth profiles. The time averaged value of $(g_1 - g_2)$ is in the order of 5% as mentioned at the end of Section 2.1. Fig. 8 shows the variation of $0.05\sigma^2_{c-k}$ for 200 randomly generated and horizontally layered models at two different depths. It is seen that the mean values are the same, 1.1 %, while the standard deviations are 0.7 % and 0.4 % for 750 m and 1500 m, respectively. Since the deeper structures consist of more layers than the shallower ones in average, the standard deviation of $0.05\sigma^2_{c-k}$ decreases with increasing depth due to the higher number of layers. On the other hand, the mean value is not effected by depth and remains as 1.1 % although both thicknesses and thermal properties of layers take considerably different values in wide ranges. Therefore, these results suggest that the homogeneous model can safely be used for the predictions of borehole heat transfer in almost all types of horizontally layered geological structures. If the typical orientation of geological layers in an application field is already known to be horizontal from geological/geophysical observations or from a borehole drilled for a thermal response test, then the homogenized approach is sufficient for engineering design of a borehole field. Analytical expressions can be used not only for the heat transfer problem of ground heat exchangers in layered geological structures but also for any problem of heat conduction through parallel layered structures.

CRediT authorship contribution statement

Sevan Karabetoglu: Formal analysis, Visualization. **Z. Fatih Ozturk:** Formal analysis, Writing - original draft. **Ayse Kaslilar:** Data curation, Visualization, Writing - review & editing. **Christopher Juhlin:** Data curation, Writing - review & editing. **Altug Sisman:** Conceptualization, Methodology, Supervision.

Declaration of Competing Interest

The authors declare that they have no known competing financial interests or personal relationships that could have appeared to influence the work reported in this paper.

Acknowledgement

The authors would like to thank the editor and two anonymous reviewers for their constructive comments, which helped us to improve the manuscript.

Appendix A

A. Simplified forms of variance functions

$\sigma^2_c, \sigma^2_k, \sigma^2_{ck}$ and σ^2_{c-k} given in Eqs. (18a)–(18d) can be rewritten even more simple forms as follows

$$\sigma_c^2 = \sum_{i=1}^{N} \tilde{z}_i \tilde{c}_i^2 - 1 = \sum_{i=1}^{N} \tilde{z}_i \left(\frac{c_i}{\bar{c}}\right)^2 - 1 = \frac{1}{\bar{c}^2} \sum_{i=1}^{N} \tilde{z}_i c_i^2 - 1 = \frac{\overline{c^2}}{\bar{c}^2} - 1 \tag{A1a}$$

$$\sigma_k^2 = \sum_{i=1}^{N} \tilde{z}_i \tilde{k}_i^2 - 1 = \sum_{i=1}^{N} \tilde{z}_i \left(\frac{k_i}{\bar{k}}\right)^2 - 1 = \frac{1}{\bar{k}^2} \sum_{i=1}^{N} \tilde{z}_i k_i^2 - 1 = \frac{\overline{k^2}}{\bar{k}^2} - 1 \tag{A1b}$$

$$\sigma_{ck}^2 = \sum_{i=1}^{N} \tilde{z}_i \tilde{c}_i \tilde{k}_i - 1 = \sum_{i=1}^{N} \tilde{z}_i \left(\frac{c_i k_i}{\bar{c}\bar{k}}\right) - 1 = \frac{\overline{ck}}{\bar{c}\bar{k}} - 1 \tag{A1c}$$

Therefore,

$$\sigma_{c-k}^2 = \sigma_k^2 + \sigma_c^2 - 2\sigma_{ck}^2 = \frac{\overline{k^2}}{\bar{k}^2} + \frac{\overline{c^2}}{\bar{c}^2} - 2\frac{\overline{ck}}{\bar{c}\bar{k}} \tag{A1d}$$

In most of the cases, differences in volumetric heat capacity of geological units are small in comparison with those in thermal conductivity, see Table 2. By considering this behavior, if we assume that c is approximately a constant quantity, then $\sigma_c^2 = \sigma_{ck}^2 = 0$ and Eq. (A1d) simplifies even further to

$$\sigma_{c-k}^2 \cong \sigma_k^2 = \frac{\overline{k^2}}{\bar{k}^2} - 1 \tag{A2}$$

In Eq. (A2), averaging processes of k and k^2 are made by considering the thicknesses of layers as weight factor defined by Eq. (A1b).

Appendix B

B. 3rd order representation of relative heat transfer rate and transferred heat energy

If the 3rd order terms of Eq. (13a) are considered, then Eq. (13b) can be expressed as

$$\widetilde{k}_i \exp\left(-\beta^2 \widetilde{t}_{\widetilde{a}} \frac{\widetilde{k}_i}{\widetilde{c}_i}\right) \approx e^{-\lambda} \left\{ \begin{array}{l} \widetilde{k}_i - \lambda\left[\left(\widetilde{k}_i - 1\right) - \left(\widetilde{c}_i - 1\right)\right] + \frac{1}{2}\left(\lambda^2 - 2\lambda\right)\left[\left(\widetilde{c}_i - 1\right)^2 - 2\left(\widetilde{k}_i - 1\right)\left(\widetilde{c}_i - 1\right) + \left(\widetilde{k}_i - 1\right)^2\right] \\ + \frac{\lambda^3}{6}\left[\left(\widetilde{c}_i - 1\right)^3 - 3\left(\widetilde{c}_i - 1\right)^2\left(\widetilde{k}_i - 1\right) + 3\left(\widetilde{c}_i - 1\right)\left(\widetilde{k}_i - 1\right)^2 - \left(\widetilde{k}_i - 1\right)^3\right] \\ -\left(\lambda^2 - \lambda\right)\left(\widetilde{c}_i - 1\right)^3 + \left(\frac{5}{2}\lambda^2 - 2\lambda\right)\left(\widetilde{c}_i - 1\right)^2\left(\widetilde{k}_i - 1\right) - \left(2\lambda^2 - \lambda\right)\left(\widetilde{c}_i - 1\right)\left(\widetilde{k}_i - 1\right)^2 + \frac{\lambda^2}{2}\left(\widetilde{k}_i - 1\right)^3 \end{array} \right\} \tag{B1}$$

where $\lambda = \beta^2 \widetilde{t}_{\widetilde{a}}$ for simplicity. By using Eq. (B1) and the following statistical parameters in Eq. (11),

$$\sigma_c^3 = \sum_{i=1}^{N} \widetilde{z}_i \left(\widetilde{c}_i - 1\right)^3 \tag{B2a}$$

$$\sigma_k^3 = \sum_{i=1}^{N} \widetilde{z}_i \left(\widetilde{k}_i - 1\right)^3 \tag{B2b}$$

$$\sigma_{cck}^3 = \sum_{i=1}^{N} \widetilde{z}_i \left(\widetilde{c}_i - 1\right)^2 \left(\widetilde{k}_i - 1\right) \tag{B2c}$$

$$\sigma_{ckk}^3 = \sum_{i=1}^{N} \widetilde{z}_i \left(\widetilde{c}_i - 1\right) \left(\widetilde{k}_i - 1\right)^2 \tag{B2d}$$

$$\sigma_{(c-k)}^3 = \sum_{i=1}^{N} \widetilde{z}_i \left[\left(\widetilde{c}_i - 1\right) - \left(\widetilde{k}_i - 1\right)\right]^3 \tag{B2e}$$

the relative heat transfer rate, $\widehat{Q}$, is expressed in 3rd order approach as

$$\widehat{Q} = 1 - \sigma_{(c-k)}^2 (g_1 - g_2) + \sigma_{(c-k)}^3 g_3 + \sigma_c^3 (g_1 - 2g_2) - \sigma_{cck}^3 (2g_1 - 5g_2) + \sigma_{ckk}^3 (g_1 - 4g_2) + \sigma_k^3 g_2 \tag{B3}$$

In a very similar way, relative heat energy transfer, $\widehat{Q}$, is obtained in 3rd order approach as follows

$$\widehat{Q} = 1 - h_2 \sigma_{c-k}^2 - h_3 \sigma_{c-k}^3 + h_2 \left(\sigma_c^3 - 2\sigma_{cck}^3 + \sigma_{ckk}^3\right) \tag{B4}$$

Appendix C. Supplementary data

Supplementary material related to this article can be found, in the online version, at doi:https://doi.org/10.1016/j.geothermics.2021.102043.

References

Abdelaziz, S.L., Ozudogru, T.Y., Olgun, C.G., Martin, J.R., 2014. Multilayer finite line source model for vertical heat exchangers. Geothermics 51, 406–416. https://doi.org/10.1016/j.geothermics.2014.03.004.

Acuña, J., 2013. Distributed Thermal Response Tests – New Insights on U-pipe and Coaxial Heat Exchangers in Groundwater-filled Boreholes, Ph.D. Thesis. KTH Royal Institute of Technology.

Asdrubali, F., Desideri, U., 2018. Handbook of Energy Efficiency in Buildings - a Life Cycle Approach. Butterworth-Heinemann. https://doi.org/10.1016/C2016-0-02638-4.

Atam, E., Helsen, L., 2016. Ground-coupled heat pumps: part 2 - Literature review and research challenges in optimal design. Renew. Sustain. Energy Rev. 54 https://doi.org/10.1016/j.rser.2015.07.009, 1886-1684.

Aydin, M., Sisman, A., 2015. Experimental and computational investigation of multi U-tube boreholes. Appl. Energy 145, 163–171. https://doi.org/10.1016/j.apenergy.2015.02.036.

Cai, W., Wang, F., Liu, J., Wang, Z., Ma, Z., 2019. Experimental and numerical investigation of heat transfer performance and sustainability of deep borehole heat exchangers coupled with ground source heat pump systems. Appl. Therm. Eng. 149, 975–986. https://doi.org/10.1016/j.applthermaleng.2018.12.094.

Eppelbaum, L., Kutasov, I., Pilchin, A., 2014. Applied Geothermics. Springer-Verlag Berlin Heidelberg. https://doi.org/10.1007/978-3-642-34023-9.

Erol, S., François, B., 2018. Multilayer analytical model for vertical ground heat exchanger with groundwater flow. Geothermics 71, 294–305. https://doi.org/10.1016/j.geothermics.2017.09.008.

Eskilson, P., 1987. Thermal Analysis of Heat Extraction Boreholes, Ph.D. Thesis. University of Lund, Lund, Sweden.

Florides, G.A., Christodoulides, P., Pouloupatis, P., 2013. Single and double U-tube ground heat exchangers in multiple-layer substrates. Appl. Energy 102, 364–373. https://doi.org/10.1016/j.apenergy.2012.07.035.

Fuchs, S., Balling, N., Forster, A., 2015. Calculation of thermal conductivity, thermal diffusivity and specific heat capacity of sedimentary rocks using petrophysical well logs. Geophys. J. Int. 203, 1977–2000. https://doi.org/10.1093/gji/ggv403.

Fujii, H., Okubo, H., Itoi, R., 2006. Thermal response tests using optical fiber thermometers. Trans. - Geotherm. Resour. Counc. 30, 545–551.

Fujii, H., Okubo, H., Nishi, K., Itoi, R., Ohyama, K., Shibata, K., 2009. An improved thermal response test for U-tube ground heat exchanger based on optical fiber thermometers. Geothermics 38, 399–406. https://doi.org/10.1016/j.geothermics.2009.06.002.

Gultekin, A., Aydin, M., Sisman, A., 2016. Thermal performance analysis of multiple borehole heat exchangers. Energy Convers. Manage. 122, 544–551. https://doi.org/10.1016/j.enconman.2016.05.086.

Hecht-Méndez, J., De Paly, M., Beck, M., Bayer, P., 2013. Optimization of energy extraction for vertical closed-loop geothermal systems considering groundwater flow. Energy Convers. Manage. 66, 1–10. https://doi.org/10.1016/j.enconman.2012.09.019.

Hu, J., 2017. An improved analytical model for vertical borehole ground heat exchanger with multiple-layer substrates and ground flow. Appl. Energy 202, 537–549. https://doi.org/10.1016/j.apenergy.2017.05.152.
Ivanova, A., Juhlin, C., Lenglera, U., Bergmanna, P., Lütha, S., Kempka, T., 2013. Impact of temperature on CO2 storage at the Ketzin site based on fluidflow simulations and seismic data. Int. J. Greenh. Gas Control. 19, 775–784. https://doi.org/10.1016/j.ijggc.2013.05.001.
Jin, G., Li, Z., Guo, S., Wu, X., Wu, W., Zhang, K., 2020. Thermal performance analysis of multiple borehole heat exchangers in multilayer geotechnical media. Energy 209, 118236. https://doi.org/10.1016/j.energy.2020.118236.
Katsura, T., Nagano, K., Takeda, S., 2008. Method of calculation of the ground temperature for multiple ground heat exchangers. Appl. Therm. Eng. 28, 1995–2004. https://doi.org/10.1016/j.applthermaleng.2007.12.013.
Kurevija, T., Krapec, V., Vulin, D., 2011. Effect of borehole array geometry and thermal interferences on geothermal heat pump system. Energy Convers. Manage. 60, 134–142. https://doi.org/10.1016/j.enconman.2012.02.012.
Labus, M., Labus, K., 2018. Thermal conductivity and diffusivity of fine-grained sedimentary rocks. J. Therm. Anal. Calorim. 132, 1669–1676. https://doi.org/10.1007/s10973-018-7090-5.
Law, Y.L.E., Dworkin, S.B., 2016. Characterization of the effects of borehole configuration and interference with long term ground temperature modelling of ground source heat pumps. Appl. Energy 179, 1032–1047. https://doi.org/10.1016/j.apenergy.2016.07.048.
Li, Y., Han, X., Xiaosong, Z., Geng, S., Li, C., 2017. Study the performance of borehole heat exchanger considering layered subsurface based on field investigations. Appl. Therm. Eng. 126, 296–304. https://doi.org/10.1016/j.applthermaleng.2017.07.109.
Li, W., Li, X., Du, R., Wang, Y., Tu, J., 2019. Experimental investigations of the heat load effect on heat transfer of ground heat exchangers in a layered subsurface. Geothermics 77, 75–82. https://doi.org/10.1016/j.geothermics.2018.08.011.
Liu, J., Wang, F., Cai, W., Wang, Z., Li, C., 2020a. Numerical investigation on the effects of geological parameters and layered subsurface on the thermal performance of medium-deep borehole heat exchanger. Renew. Energy 149, 384–399. https://doi.org/10.1016/j.renene.2019.11.158.
Liu, Z., Li, R., Wang, D., Li, H., Shi, L., 2020b. Multilayer quasi-three-dimensional model for the heat transfer inside the borehole wall of a vertical ground heat exchanger. Geothermics 83, 101711. https://doi.org/10.1016/j.geothermics.2019.101711.
Loveridge, F., Powrie, W., 2014. G-Functions for multiple interacting pile heat exchangers. Energy 64, 747–757. https://doi.org/10.1016/j.energy.2013.11.014.
Luo, J., Rohn, J., Bayer, M., Priess, A., Xiang, W., 2014. Analysis on performance of borehole heat exchanger in a layered subsurface. Appl. Energy 123, 55–57. https://doi.org/10.1016/j.apenergy.2014.02.044.
Luo, Y., Guo, H., Meggers, F., Zhang, L., 2019. Deep coaxial borehole heat exchanger: analytical modeling and thermal analysis. Energy 185, 1298–1313. https://doi.org/10.1016/j.energy.2019.05.228.
Makasis, N., Narsilio, G.A., Bidarmaghz, A., Johnston, I.W., 2018. Ground-source heat pump systems: the effect of variable pipe separation in ground heat exchangers. Comput. Geotech. 100, 97–109. https://doi.org/10.1016/j.compgeo.2018.02.010.
Meng, B., Vienken, T., Kolditz, O., Shao, H., 2018. Modeling the groundwater temperature response to extensive operation of ground source heat pump systems: a case study in Germany. Energy Proc. 152, 971–977. https://doi.org/10.1016/j.egypro.2018.09.102.
Mogensen, P., 1983. Fluid to duct wall heat transfer in duct system heat storage. In: Proceedings, International Conference on Surface Heat Storage in Theory and Practice. Sweden, Stockholm.
Morchio, S., Fossa, M., 2019. Thermal modeling of deep borehole heat exchangers for geothermal applications in densely populated urban areas. Therm. Sci. Eng. Prog. 13, 100363 https://doi.org/10.1016/j.tsep.2019.100363.
Ozisik, M.N., 1993. Heat Conduction. John Wiley & Sons Inc., New York, NY, USA, p. 112.
Pan, A., McCartney, J.S., Lu, L., You, T., 2020. A novel analytical multilayer cylindrical heat source model for vertical ground heat exchangers installed in layered ground. Energy 200, 117545. https://doi.org/10.1016/j.energy.2020.117545.
Rees, S.J., 2016. Advances in Ground-Source Heat Pump Systems, Advances in Ground-Source Heat Pump Systems. Woodhead, Duxford UK. https://doi.org/10.1016/C2014-0-03840-3.
Renaud, T., Verdin, P., Falcone, G., 2019. Numerical simulation of a deep borehole heat exchanger in the Krafla geothermal system. Int. J. Heat Mass Transf. 143, 118496 https://doi.org/10.1016/j.ijheatmasstransfer.2019.118496.
Sakata, Y., Katsura, T., Nagano, K., 2018. Multilayer-concept thermal response test: measurement and analysis methodologies with a case study. Geothermics 71, 178–186. https://doi.org/10.1016/j.geothermics.2017.09.004.
Schärli, U., Rybach, L., 2001. Determination of specific heat capacity on rock fragments. Geothermics 30, 93–110. https://doi.org/10.1016/S0375-6505(00)00035-3.
Serrano, S., Ürge-Vorsatz, D., Barreneche, C., Palacios, A., Cabeza, L.F., 2017. Heating and cooling energy trends and drivers in Europe. Energy 119, 425–434. https://doi.org/10.1016/j.energy.2016.12.080.
Spitler, J.D., Gehlin, S.E.A., 2015. Thermal response testing for ground source heat pump systems - an historical review. Renew. Sustain. Energy Rev. 50, 1125–1137. https://doi.org/10.1016/j.rser.2015.05.061.
Ürge-Vorsatz, D., Cabeza, L.F., Serrano, S., Barreneche, C., Petrichenko, K., 2015. Heating and cooling energy trends and drivers in buildings. Renew. Sustain. Energy Rev. 41, 85–98. https://doi.org/10.1016/j.rser.2014.08.039.
Yang, H., Cui, P., Fang, Z., 2010. Vertical-borehole ground-coupled heat pumps: a review of models and systems. Appl. Energy 87, 16–27. https://doi.org/10.1016/j.apenergy.2009.04.038.
Yuan, Y., Cao, X., Wang, J., Sun, L., 2016. Thermal interaction of multiple ground heat exchangers under different intermittent ratio and separation distance. Appl. Therm. Eng. 108, 277–286. https://doi.org/10.1016/j.applthermaleng.2016.07.120.
Zanchini, E., Lazzari, S., Priarone, A., 2012. Long-term performance of large borehole heat exchanger fields with unbalanced seasonal loads and groundwater flow. Energy 38, 66–77. https://doi.org/10.1016/j.energy.2011.12.038.